Finite Volume/Element Discretization on Unstructured Meshes of the Multiscale Formulation of the Large Eddy Simulation Method and Application to Vortex Shedding

B. Koobus, C. Farhat

INRIA

INSTITUT NATIONAL DE RECHERCHE EN INFORMATIQUE ET EN AUTOMATIQUE

Finite Volume/Element Discretization on Unstructured Meshes of the Multiscale Formulation of the Large Eddy Simulation Method and Application to Vortex Shedding

B. Koobus - C. Farhat

N° 4722

February, 2003

THÈME 4

ISSN 0249-6399 ISRN INRIA/RR--4722--FR+ENG

INRIA
SOPHIA ANTIPOLIS

Finite Volume/Element Discretization on Unstructured Meshes of the Multiscale Formulation of the Large Eddy Simulation Method and Application to Vortex Shedding

B. Koobus* - C. Farhat†

Thème 4 — Simulation et optimisation
de systèmes complexes
Projet Smash

Rapport de recherche n° 4722 — February, 2003 — 25 pages

Abstract: A finite volume/element discretization on tetrahedral meshes of the variational multiscale formulation of large eddy simulations is proposed for turbulent compressible flows. This discretization features an economical procedure based on agglomeration for separating a priori the scales, a corresponding projector for eliminating the small scales from the system of equations, and an effective control of the numerical dissipation induced by upwinding. The resulting LES method is validated with the three-dimensional numerical simulation of a low-speed flow past a square cylinder at $M_\infty = 0.1$ and $Re = 22{,}000$, and various comparisons with experimental data.

Key-words: LES, compressible flows, variational multiscale, unstructured meshes, agglomeration, vortex shedding.

* Université de Montpellier II, Dept Mathématiques, CC 051, 34095 MONTPELLIER Cedex 5, France, et INRIA Sophia-Antipolis
† Department of Aerospace Engineering Sciences, University of Colorado at Boulder, Campus Box 429, Boulder, CO 80309-0429, USA

Unité de recherche INRIA Sophia Antipolis
2004, route des Lucioles, BP 93, 06902 Sophia Antipolis Cedex (France)
Téléphone : +33 4 92 38 77 77 — Télécopie : +33 4 92 38 77 65

Discrétisation par EF/VF sur maillages non structurés de la formulation multiéchelles de la LES et application à un écoulement avec développement de tourbillons

Résumé : Une discrétisation Eléments Finis/Volumes Finis sur maillages tétraèdriques de la formulation multiéchelles de la Simulation des Grandes Echelles (LES) est proposée pour le calcul d'écoulements compressibles turbulents. Cette discrétisation utilise une procédure économique qui repose sur une méthode d'agglomération pour séparer à priori les échelles, un projecteur pour éliminer les petites échelles du système d'équations, et un contrôle de la dissipation numérique due au décentrage. La méthode LES résultante est validée par la simulation numérique tri-dimensionnelle d'un écoulement subsonique autour d'un cylindre carré à $M_\infty = 0.1$ et $Re = 22000$, et des comparaisons avec des données expérimentales sont présentées.

Mots-clés : LES, écoulements compressibles, formulation variationnelle multiéchelles, maillages non structurés, agglomération, développement de tourbillons.

1 Introduction

For turbulent flows, large eddy simulations (LES) are an interesting compromise between accurate but not always computationally feasible direct numerical simulations (DNS), and more economical but not always sufficiently accurate Reynolds averaged Navier-Stokes models. The main idea behind LES is to resolve the large-scale features of a turbulent flow, and model the subgrid-scale stresses which represent the effect of the unresolved scales on the resolved ones. To this effect, many different LES models have been proposed in the literature. The original Smagorinsky eddy viscosity model [1] has traditionally played a dominant part, either alone, or as part of another scheme. However, for some flows, this model can exhibit some shortcomings such as a wrong asymptotic behavior near walls, an excessive dissipation in the presence of large coherent structures, and the inability to allow for backscatter. To remedy these issues, several modifications of the Smagorinsky model have been proposed. Among these stands out the dynamic subgrid-scale model [2, 3, 6] in which the Smagorinsky constant-coefficient is considered as a function of space and time. In most cases but a few flow configurations, this dynamic model appears to improve the fidelity of LES (see for example [4, 5] for a recent application). However, for unstructured meshes, it can be computationally expensive.

A new approach to LES based on a variational multiscale (VMS) framework was recently introduced by Hughes and his co-workers [7, 8, 9]. The VMS-LES differs from the traditional LES in a number of ways. In this new approach, one does not filter the Navier-Stokes equations but uses instead a variational projection. This is an important difference because as performed in the traditional LES, filtering works well with periodic boundary conditions but raises mathematical issues in wall-bounded flows. The variational projection avoids these issues. Furthermore, the VMS-LES method separates the scales *a priori* — that is, before the simulation is started. And most importantly, it models the effect of the unresolved scales only in the equations representing the smallest resolved scales, and not in the equations for the large scales. Consequently, in the VMS-LES, energy is extracted from the fine resolved scales by a traditional model such as the Smagorinsky eddy viscosity model, but no energy is directly extracted from the large structures in the flow. For this reason, one can reasonably hope to obtain a better behavior near walls, and less dissipation in the presence of large coherent structures.

The initial development of the VMS-LES method focused on regular grids and spectral discretizations as in this case the separation a priori of the scales is simple to achieve, for example, by introducing a frequency cutoff [7, 8, 9]. For finite element approximations, a hierarchical basis approach [10] and an alternative method based on cell agglomeration [11] were recently proposed for separating a priori the coarse and fine scales. In most cases, the VMS-LES method was applied mainly to homogeneous isotropic incompressible turbulence, and recently to incompressible turbulent channel flows, for which it demonstrated an improvement over the traditional LES method [8, 9].

The objectives of this paper are two fold. It proposes a general approach for discretizing the VMS-LES method on unstructured grids in order to pave the way for applications with complex geometries. This approach, which was first outlined in [11], is equally applicable

to the finite volume (FV) and finite element (FE) methods, and to incompressible as well as compressible flows. Its key elements are an economical projector for eliminating the fine scales from the system of equations which is based on agglomeration, an effective strategy for controling the numerical dissipation induced by upwinding that features a sixth-order viscosity [13, 18], and explicit as well as semi-implicit frameworks for time-integrating the governing semi-discrete equations. The paper also reports on the application of the VMS-LES method to the prediction of a vortex shedding flow for which experimental data is available. To this effect, the remainder of this paper is organized as follows.

In Section 2, the multi-scale variational formulation is applied to the compressible Navier-Stokes equations and the semi-discretization method adopted in this work is outlined. A procedure based on agglomeration for separating a priori the coarse and fine scales of a turbulent flow on unstructured tetrahedral meshes is presented in Section 3. Modeling of the subgrid scales is discussed in Section 4. In Section 5, the semi-discretization method chosen for this work is discussed in further details. In particular, an upwind stabilization term involving a sixth-order spatial viscosity is introduced in order to minimize the competition between numerical and modeled dissipations. Time-discretization is addressed in Section 6. The resulting VMS-LES method is applied in Section 7 to the simulation of a vortex shedding dominated flow past a three-dimensional square cylinder. The obtained numerical results are contrasted with those predicted by various implementations of the classical and dynamical LES method and compared with experimental data. Finally, concluding remarks are offered in Section 8.

2 Variational multiscale formulation of the compressible Navier-Stokes equations

The conservative form of the compressible Navier-Stokes equations is given by

$$\left\{\begin{array}{ll} \dfrac{\partial \rho}{\partial t} + \nabla.(\rho \mathbf{u}) & = 0 \\ \dfrac{\partial \rho \mathbf{u}}{\partial t} + \nabla.(\rho \mathbf{u} \otimes \mathbf{u}) & = -\nabla P + \nabla.\sigma \\ \dfrac{\partial E}{\partial t} + \nabla.[(E+P)\mathbf{u}] & = \nabla.(\sigma \mathbf{u}) + \nabla.(\lambda \nabla T) \end{array}\right.$$

where $\rho, \mathbf{u}, P, \sigma, E, \lambda$, and T are respectively the density, velocity, pressure, viscous stress tensor, total energy, thermal conductivity, and temperature of the flow. The viscous stress tensor is given by $\sigma_{ij} = \mu(2\mathbf{S}_{ij} - \frac{2}{3}\mathbf{S}_{kk}\delta_{ij})$ where μ is the viscosity and $\mathbf{S}_{ij} = \frac{1}{2}(\frac{\partial \mathbf{u}_i}{\partial \mathbf{x}_j} + \frac{\partial \mathbf{u}_j}{\partial \mathbf{x}_i})$. The total energy E is given by $E = \rho C_v T + \frac{1}{2}\rho \mathbf{u}.\mathbf{u}$ where C_v is the specific heat at constant volume, and the density, pressure and temperature are assumed to be related by the state law for a perfect gas $P = \rho RT$. For simplicity, μ and λ are assumed to be constant.

Furthermore, it is assumed here that:

- The bounded flow domain Ω is to be discretized by a tedrahedral mesh from which a dual mesh defined by cells or control volumes can be derived.
- The convective fluxes are to be treated by a FV method in which a variable w is first approximated by a constant in each control volume. This can be written as $w = \sum_i w_i \mathcal{X}_i$ where $\mathcal{X}_i$ is the characteristic function corresponding to the control volume C_i associated with node i, and w_i denotes the constant value of w in this control volume. Next, this first-order approximation is transformed into a sixth-order viscosity semi-discretization [13, 18] by a MUSCL [14, 15] approach that is specified in Section 5.
- The diffusive fluxes are to be treated by a FE method in which a flow variable w is approximated by a continuous piecewise linear function. This can be written as $w = \sum_i w_i \Phi_i$ where Φ_i is the P1 shape function associated with node i, and w_i denotes the value of w at this node.

However, it is noted that all methodologies presented in this paper equally apply to the case where both the convective and diffusive fluxes are approximated by a (stabilized) FE method or a FV method.

The semi-discretization of the compressible Navier-Stokes equations (2) by a mixed FV/FE method with mass lumping leads to a system of equations of the form

$$\left\{ \begin{array}{ll} A(\mathcal{X}_i, \mathbf{W}) & = 0 \\ \mathbf{B}(\mathcal{X}_i, \Phi_i, \mathbf{W}) & = \mathbf{0} \\ C(\mathcal{X}_i, \Phi_i, \mathbf{W}) & = 0 \end{array} \right. \tag{1}$$

where $\mathbf{W} = (\rho, \mathbf{u}, T)^t$,

$$\left\{ \begin{array}{lll} A(\mathcal{X}_i, \mathbf{W}) & = \displaystyle\int_\Omega \frac{\partial \rho}{\partial t} \mathcal{X}_i \, d\Omega & + \displaystyle\int_{\partial Sup\mathcal{X}_i} \rho \mathbf{u}.\mathbf{n} \mathcal{X}_i \, d\Gamma \\ \mathbf{B}(\mathcal{X}_i, \Phi_i, \mathbf{W}) & = \displaystyle\int_\Omega \frac{\partial \rho \mathbf{u}}{\partial t} \mathcal{X}_i \, d\Omega & + \displaystyle\int_{\partial Sup\mathcal{X}_i} \rho \, \mathbf{u} \otimes \mathbf{u} \, \mathbf{n} \mathcal{X}_i \, d\Gamma \\ & + \displaystyle\int_{\partial Sup\mathcal{X}_i} P \mathbf{n} \mathcal{X}_i \, d\Gamma & + \displaystyle\int_\Omega \sigma \nabla \Phi_i \, d\Omega \\ C(\mathcal{X}_i, \Phi_i, \mathbf{W}) & = \displaystyle\int_\Omega \frac{\partial E}{\partial t} \mathcal{X}_i \, d\Omega & + \displaystyle\int_{\partial Sup\mathcal{X}_i} (E + P) \mathbf{u}.\mathbf{n} \mathcal{X}_i \, d\Gamma \\ & + \displaystyle\int_\Omega \sigma \mathbf{u}.\nabla \Phi_i \, d\Omega & + \displaystyle\int_\Omega \lambda \nabla T.\nabla \Phi_i \, d\Omega \end{array} \right.$$

$\partial Sup\mathcal{X}_i$ denotes the boundary of the support of $\mathcal{X}_i$, and $\mathbf{n}$ is the outward normal to this support.

Let $\mathcal{V}_{FV}$ and $\mathcal{V}_{FE}$ denote respectively the space spanned by the the characteristic functions $\{\mathcal{X}_k\}$, and that spanned by the P1 shape functions $\{\Phi_k\}$. In order to separate a priori the coarse and fine scales, these spaces are decomposed as follows

$$\mathcal{V}_{FV} = \overline{\mathcal{V}}_{FV} \oplus \mathcal{V}'_{FV}, \tag{2}$$

and

$$\mathcal{V}_{FE} = \overline{\mathcal{V}}_{FE} \oplus \mathcal{V}'_{FE}. \tag{3}$$

Here and throughout the remainder of this paper, the overline designates a coarse scale, and the $'$ superscript designates a fine scale. Hence, consistently with Eqs. (2,3), $\mathbf{W}$ is decomposed into a coarse scale $\overline{\mathbf{W}}$ and a fine scale $\mathbf{W}'$

$$\mathbf{W} = \overline{\mathbf{W}} + \mathbf{W}'. \tag{4}$$

From the decompositions (2) and (3) follows the decomposition of problem (1) into the two following subproblems

$$\left\{ \begin{array}{ll} A(\overline{\mathcal{X}}_i, \overline{\mathbf{W}} + \mathbf{W}') & = 0 \\ \mathbf{B}(\overline{\mathcal{X}}_i, \overline{\Phi}_i, \overline{\mathbf{W}} + \mathbf{W}') & = \mathbf{0} \\ C(\overline{\mathcal{X}}_i, \overline{\Phi}_i, \overline{\mathbf{W}} + \mathbf{W}') & = 0 \end{array} \right. \tag{5}$$

and

$$\left\{ \begin{array}{ll} A(\mathcal{X}'_i, \overline{\mathbf{W}} + \mathbf{W}') & = 0 \\ \mathbf{B}(\mathcal{X}'_i, \Phi'_i, \overline{\mathbf{W}} + \mathbf{W}') & = \mathbf{0} \\ C(\mathcal{X}'_i, \Phi'_i, \overline{\mathbf{W}} + \mathbf{W}') & = 0 \end{array} \right. \tag{6}$$

where

$$\begin{array}{lll} A(\mathcal{X}_i, \overline{\mathbf{W}} + \mathbf{W}') & = A(\mathcal{X}_i, \overline{\mathbf{W}}) \; + \; A_1(\mathcal{X}_i, \overline{\mathbf{W}}, \mathbf{W}'), & \\ A_1(\mathcal{X}_i, \overline{\mathbf{W}}, \mathbf{W}') & = \displaystyle\int_\Omega \frac{\partial \rho'}{\partial t} \mathcal{X}_i \, d\Omega \; + \; \int_{\partial Sup \mathcal{X}_i} \rho' \overline{\mathbf{u}}.\mathbf{n} \mathcal{X}_i \, d\Gamma \; + \; \int_{\partial Sup \mathcal{X}_i} \rho \mathbf{u}'.\mathbf{n} \mathcal{X}_i \, d\Gamma, & \end{array} \tag{7}$$

$$\begin{array}{lll} \mathbf{B}(\mathcal{X}_i, \Phi_i, \overline{\mathbf{W}} + \mathbf{W}') & = \mathbf{B}(\mathcal{X}_i, \Phi_i, \overline{\mathbf{W}}) \; + \; \mathbf{B}_1(\mathcal{X}_i, \Phi_i, \overline{\mathbf{W}}, \mathbf{W}') \; + \; \mathbf{B}_2(\mathcal{X}_i, \overline{\mathbf{W}}, \mathbf{W}'), & \\ \mathbf{B}_1(\mathcal{X}_i, \Phi_i, \overline{\mathbf{W}}, \mathbf{W}') & = \displaystyle\int_\Omega \frac{\partial \rho \mathbf{u}'}{\partial t} \mathcal{X}_i \, d\Omega \; + \; \int_\Omega \frac{\partial \rho' \overline{\mathbf{u}}}{\partial t} \mathcal{X}_i \, d\Omega & \\ & + \displaystyle\int_{\partial Sup \mathcal{X}_i} \rho \, \mathbf{u}' \otimes \overline{\mathbf{u}} \, \mathbf{n} \mathcal{X}_i \, d\Gamma \; + \; \int_{\partial Sup \mathcal{X}_i} \rho \, \overline{\mathbf{u}} \otimes \mathbf{u}' \, \mathbf{n} \mathcal{X}_i \, d\Gamma & \\ & + \displaystyle\int_{\partial Sup \mathcal{X}_i} \rho' \, \overline{\mathbf{u}} \otimes \overline{\mathbf{u}} \, \mathbf{n} \mathcal{X}_i \, d\Gamma \; + \; \int_{\partial Sup \mathcal{X}_i} (P - \overline{\rho} R \overline{T}) \mathbf{n} \mathcal{X}_i \, d\Gamma & \\ & + \displaystyle\int_\Omega \sigma' \nabla \Phi_i \, d\Omega, & \\ \mathbf{B}_2(\mathcal{X}_i, \overline{\mathbf{W}}, \mathbf{W}') & = \displaystyle\int_{\partial Sup \mathcal{X}_i} \rho \, \mathbf{u}' \otimes \mathbf{u}' \, \mathbf{n} \mathcal{X}_i \, d\Gamma, & \end{array} \tag{8}$$

and

$$
\begin{aligned}
C(\mathcal{X}_i,\Phi_i,\overline{\mathbf{W}}+\mathbf{W}') &= C(\mathcal{X}_i,\Phi_i,\overline{\mathbf{W}}) \;+\; C_1(\mathcal{X}_i,\Phi_i,\overline{\mathbf{W}},\mathbf{W}') \;+\; C_2(\mathcal{X}_i,\Phi_i,\overline{\mathbf{W}},\mathbf{W}'),\\
C_1(\mathcal{X}_i,\Phi_i,\overline{\mathbf{W}},\mathbf{W}') &= \int_\Omega \frac{\partial(E-\overline{\rho}C_v\overline{T}-\frac{1}{2}\overline{\rho}\,\overline{\mathbf{u}}.\overline{\mathbf{u}})}{\partial t}\mathcal{X}_i\,d\Omega\\
&\quad+\int_{\partial Sup\mathcal{X}_i}(E-\overline{\rho}C_v\overline{T}-\frac{1}{2}\overline{\rho}\,\overline{\mathbf{u}}.\overline{\mathbf{u}}+P-\overline{\rho}R\overline{T})\overline{\mathbf{u}}.\mathbf{n}\mathcal{X}_i\,d\Gamma\\
&\quad+\int_{\partial Sup\mathcal{X}_i}(\overline{\rho}C_v\overline{T}+\frac{1}{2}\overline{\rho}\,\overline{\mathbf{u}}.\overline{\mathbf{u}}+\overline{\rho}R\overline{T})\mathbf{u}'.\mathbf{n}\mathcal{X}_i\,d\Gamma\\
&\quad+\int_\Omega \overline{\sigma}\mathbf{u}'.\nabla\Phi_i\,d\Omega \;+\; \int_\Omega \sigma'\overline{\mathbf{u}}.\nabla\Phi_i\,d\Omega \;+\; \int_\Omega \lambda\nabla T'.\nabla\Phi_i\,d\Omega,\\
C_2(\mathcal{X}_i,\Phi_i,\overline{\mathbf{W}},\mathbf{W}') &= \int_{\partial Sup\mathcal{X}_i}(E-\overline{\rho}C_v\overline{T}-\frac{1}{2}\overline{\rho}\,\overline{\mathbf{u}}.\overline{\mathbf{u}}+P-\overline{\rho}R\overline{T})\mathbf{u}'.\mathbf{n}\mathcal{X}_i\,d\Gamma\\
&\quad+\int_\Omega \sigma'\mathbf{u}'.\nabla\Phi_i\,d\Omega.
\end{aligned}
\tag{9}
$$

Hence, Eqs. (5,6) can be re-written as

$$
\left\{\begin{array}{ll}
A(\overline{\mathcal{X}}_i,\overline{\mathbf{W}}) \;+\; A_1(\overline{\mathcal{X}}_i,\overline{\mathbf{W}},\mathbf{W}') & =0\\
\mathbf{B}(\overline{\mathcal{X}}_i,\overline{\Phi}_i,\overline{\mathbf{W}}) \;+\; \mathbf{B}_1(\overline{\mathcal{X}}_i,\overline{\Phi}_i,\overline{\mathbf{W}},\mathbf{W}') \;+\; \displaystyle\int_{\partial Sup\overline{\mathcal{X}}_i}\rho\,\mathbf{u}'\otimes\mathbf{u}'\,\mathbf{n}\overline{\mathcal{X}}_i\,d\Gamma & =\mathbf{0}\\
C(\overline{\mathcal{X}}_i,\overline{\Phi}_i,\overline{\mathbf{W}}) \;+\; C_1(\overline{\mathcal{X}}_i,\overline{\Phi}_i,\overline{\mathbf{W}},\mathbf{W}') & \\
+\displaystyle\int_{\partial Sup\overline{\mathcal{X}}_i}(E+\overline{\rho}C_v\overline{T}-\frac{1}{2}\overline{\rho}\,\overline{\mathbf{u}}.\overline{\mathbf{u}}+P-\overline{\rho}R\overline{T})\mathbf{u}'.\mathbf{n}\overline{\mathcal{X}}_i\,d\Gamma \;+\; \int_\Omega\sigma'\mathbf{u}'.\nabla\overline{\Phi}_i d\Omega & =0
\end{array}\right.
\tag{10}
$$

and

$$
\left\{\begin{array}{ll}
A(\mathcal{X}_i',\overline{\mathbf{W}}) \;+\; A_1(\mathcal{X}_i',\overline{\mathbf{W}},\mathbf{W}') & =0\\
\mathbf{B}(\mathcal{X}_i',\Phi_i',\overline{\mathbf{W}}) \;+\; \mathbf{B}_1(\mathcal{X}_i',\Phi_i',\overline{\mathbf{W}},\mathbf{W}') & \\
+\displaystyle\int_{\partial Sup\mathcal{X}_i}\rho\,\mathbf{u}'\otimes\mathbf{u}'\,\mathbf{n}\mathcal{X}_i\,d\Gamma \;-\; \int_{\partial Sup\overline{\mathcal{X}}_i}\rho\,\mathbf{u}'\otimes\mathbf{u}'\,\mathbf{n}\overline{\mathcal{X}}_i\,d\Gamma & =\mathbf{0}\\
C(\mathcal{X}_i',\overline{\Phi}_i,\overline{\mathbf{W}}) \;+\; C_1(\mathcal{X}_i',\Phi_i',\overline{\mathbf{W}},\mathbf{W}') & \\
+\displaystyle\int_{\partial Sup\mathcal{X}_i}(E-\overline{\rho}C_v\overline{T}-\frac{1}{2}\overline{\rho}\,\overline{\mathbf{u}}.\overline{\mathbf{u}}+P-\overline{\rho}R\overline{T})\mathbf{u}'.\mathbf{n}\mathcal{X}_i\,d\Gamma & \\
-\displaystyle\int_{\partial Sup\overline{\mathcal{X}}_i}(E-\overline{\rho}C_v\overline{T}-\frac{1}{2}\overline{\rho}\,\overline{\mathbf{u}}.\overline{\mathbf{u}}+P-\overline{\rho}R\overline{T})\mathbf{u}'.\mathbf{n}\overline{\mathcal{X}}_i\,d\Gamma & \\
+\displaystyle\int_\Omega\sigma'\mathbf{u}'.\nabla\Phi_i'\,d\Omega & =0
\end{array}\right.
\tag{11}
$$

Eqs. (10) govern the coarse scales, and Eqs. (11) govern the fine scales. However, these sets of equations are coupled. Next, a mechanism is introduced for separating a priori these scales.

3 Separation a priori of the scales

As in [7], the main idea here is to define $\overline{\mathbf{W}}$ as a projection of $\mathbf{W}$ onto $\overline{\mathcal{V}}_{FE}$ so that

$$\overline{\mathbf{W}} = P(\mathbf{W}) \tag{12}$$

and

$$\mathbf{W}' = (I - P)(\mathbf{W}). \tag{13}$$

Defining a simple and yet effective projector P is the main objective of this section.

3.1 Cell agglomeration

For any given tetrahedral mesh, a corresponding dual mesh defined by cells or control volumes can always be derived. Such a dual mesh can be partitioned into macro-cells by a process known as agglomeration [16]. This process is graphically depicted in Fig. 1 for the two-dimensional case.

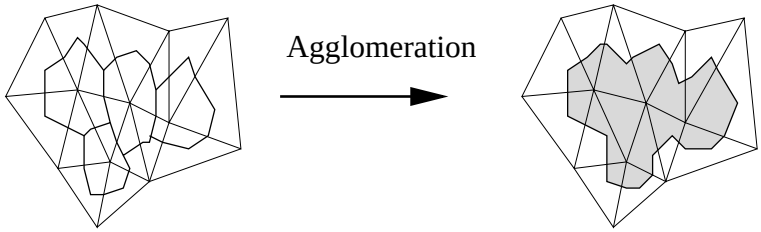

Figure 1: Unstructured mesh, dual mesh, and agglomeration of some cells of the dual mesh into a macro-cell (two-dimensional case)

Given an agglomeration into macro-cells, the idea then is to define the coarse scale component $\overline{\mathbf{W}} = P(\mathbf{W})$, in the diffusive terms, as the average of $\mathbf{W}$ in the macro-cells in the following sense

$$\overline{\mathbf{W}} = P(\sum_k \Phi_k \mathbf{W}_k) = \sum_k \Phi_k \widetilde{\mathbf{W}}_k \tag{14}$$

where

$$\widetilde{\mathbf{W}}_k = \frac{\sum_{j \in I_k} Vol(C_j)\mathbf{W}_j}{\sum_{j \in I_k} Vol(C_j)}, \tag{15}$$

C_j is the cell around the vertex j, $Vol(C_j)$ denotes its volume, $I_k = \{j \ / \ C_j \subset C_{m(k)}\}$, and $C_{m(k)}$ denotes the macro-cell containing the cell C_k.

>From Eq. (14) and Eq. (15) it follows that $\overline{\mathbf{W}}$ can also be written as

$$\overline{\mathbf{W}} = \sum_k \overline{\Phi}_k \mathbf{W}_k \tag{16}$$

where

$$\overline{\Phi}_k = \frac{Vol(C_k)}{\sum_{j \in I_k} Vol(C_j)} \sum_{j \in I_k} \Phi_j. \tag{17}$$

Given the properties of the P1 shape functions Φ_k, it follows that the coarse scale component $\overline{\mathbf{W}}$ is approximated here by a continuous function which is constant in each tetrahedron contained in a macro-cell, has the same constant value in all the tetrahedra contained in the same macro-cell, and is linear in the tetrahedra shared by at least two macro-cells. In other words, $\overline{\mathbf{W}}$ can be viewed as a piecewise constant function with linear connections between its constant stages (see Fig. 2 for a one-dimensional representation).

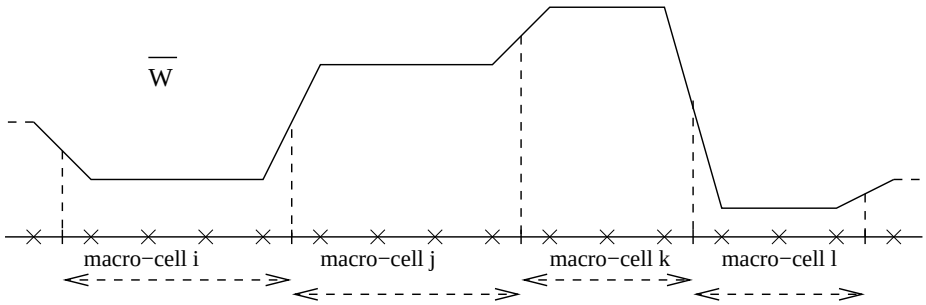

Figure 2: One-dimensional representation of a coarse scale component $\overline{\mathbf{W}}$

It also follows that

$$\mathbf{W}' = \mathbf{W} - \overline{\mathbf{W}} = \sum_k \Phi_k (\mathbf{W}_k - \widetilde{\mathbf{W}}_k) = \sum_k \Phi'_k \mathbf{W}_k = \sum_k (\Phi_k - \overline{\Phi}_k) \mathbf{W}_k. \tag{18}$$

The same averaging procedure outlined above can be applied to define the coarse scale component $\overline{\mathbf{W}} = P(\mathbf{W})$ in the convective terms, in which case Φ_k is replaced by $\mathcal{X}_k$. Hence, for the convective terms, P is defined by

$$P(\mathbf{W}) = \sum_k \left(\frac{Vol(C_k)}{\sum_{j \in I_k} Vol(C_j)} \sum_{j \in I_k} \mathcal{X}_j \right) \mathbf{W}_k \tag{19}$$

and for the diffusive terms, P is defined by

$$P(\mathbf{W}) = \sum_k \left(\frac{Vol(C_k)}{\sum_{j \in I_k} Vol(C_j)} \sum_{j \in I_k} \Phi_j \right) \mathbf{W}_k. \tag{20}$$

The reader can check that in both cases, P verifies $P^2 = P$ and therefore is a projector.

This completes the definition of the decompositions $\mathcal{V}_{FV} = \overline{\mathcal{V}}_{FV} \oplus \mathcal{V}'_{FV}$ and $\mathcal{V}_{FE} = \overline{\mathcal{V}}_{FE} \oplus \mathcal{V}'_{FE}$, where $\overline{\mathcal{V}}_{FV}$ ($\overline{\mathcal{V}}_{FE}$) denotes the space of approximation of the coarse scales spanned by the functions $\{\overline{\mathcal{X}}_k\}$ ($\{\overline{\Phi}_k\}$), and $\mathcal{V}'_{FV}$ ($\mathcal{V}'_{FE}$) denotes the space of approximation of the fine scales spanned by the functions $\{\mathcal{X}'_k\}$ ($\{\Phi'_k\}$). If n is the total number of nodes in the given mesh and N is the total number of macro-cells defined by the agglomeration, then the dimension of each of $\overline{\mathcal{V}}_{FV}$ and $\overline{\mathcal{V}}_{FE}$ is N, and that of each of $\mathcal{V}'_{FV}$ and $\mathcal{V}'_{FE}$ is $n - N$.

4 Modeling of the subgrid scales

In Eqs. (11), the quantity

$$\int_{\partial Sup \mathcal{X}_i} \rho\, \mathbf{u}' \otimes \mathbf{u}'\, \mathbf{n} \mathcal{X}_i \; d\Gamma - \int_{\partial Sup \overline{\mathcal{X}}_i} \rho\, \mathbf{u}' \otimes \mathbf{u}'\, \mathbf{n} \overline{\mathcal{X}}_i \; d\Gamma$$

plays the role of the difference between the unfiltered and filtered tensor products of velocity fluctuations ($\rho \mathbf{u}' \otimes \mathbf{u}' - \overline{\rho \mathbf{u}' \otimes \mathbf{u}'}$). Hence, this quantity can be viewed as the the fine scales' Reynolds stress.

Also in Eqs. (11), the quantity

$$\begin{aligned} \int_{\partial Sup \mathcal{X}_i} (E - \overline{\rho} C_v \overline{T} \quad & -\frac{1}{2} \overline{\rho}\, \overline{\mathbf{u}}.\overline{\mathbf{u}} + P - \overline{\rho} R \overline{T}) \mathbf{u}'.\mathbf{n} \mathcal{X}_i \; d\Gamma \\ & - \int_{\partial Sup \overline{\mathcal{X}}_i} (E - \overline{\rho} C_v \overline{T} - \frac{1}{2} \overline{\rho}\, \overline{\mathbf{u}}.\overline{\mathbf{u}} + P - \overline{\rho} R \overline{T}) \mathbf{u}'.\mathbf{n} \overline{\mathcal{X}}_i \; d\Gamma \end{aligned} \tag{21}$$

is the equivalent of the difference between the unfiltered and filtered products of enthalpy and velocity fluctuations ($(E' + P')\mathbf{u}' - \overline{(E' + P')\mathbf{u}'}$). Hence, this quantity can be viewed as the fine scales' Reynolds enthalpy flux.

The Reynolds stress generates the rapidly fluctuating fine scales that are dissipated by molecular viscosity. Because it cannot be represented accurately in the discrete case — unless all scales are resolved by means of DNS — and not because of the standard closure issue, this indirect effect on energy dissipation is modeled here by the compressible generalization of the Smagorinsky eddy viscosity model involving only the fine scales. Consequently, the term

$$\int_\Omega \tau' \nabla \Phi' \; d\Omega$$

is added to the fine scale momentum equation in Eqs. (11). Here, $\tau'_{ij} = \mu'_t(2S'_{ij} - \frac{2}{3}S'_{kk}\delta_{ij})$, $S'_{ij} = \frac{1}{2}(\frac{\partial \mathbf{u}'_i}{\partial \mathbf{x}_j} + \frac{\partial \mathbf{u}'_j}{\partial \mathbf{x}_i})$, $\mu'_t = \overline{\rho}(C'_s\Delta')^2|S'|$, $|S'| = \sqrt{2S'_{ij}S'_{ij}}$, $C'_s = 0.1$, and Δ' denotes the local grid size. In this work, Δ' is set in each tetrahedron T_l to its volume to the power one third

$$\Delta'_l = Vol(\mathrm{T}_l)^{\frac{1}{3}}. \tag{22}$$

Likewise, the Reynolds enthalpy flux is modeled here by an analogy with the Smagorinsky eddy viscosity model involving only the fine scales. More specifically, the following term

$$\int_\Omega \frac{C_p\mu'_t}{Pr_t}\nabla T'.\nabla\Phi'_i \; d\Omega$$

is added to the fine scales energy equation in Eqs. (11). Here, C_p is the specific heat at constant pressure and Pr_t is the subgrid scale Prandtl number which is assumed to be constant.

On the other hand, the term $\displaystyle\int_\Omega \sigma'\mathbf{u}'.\nabla\Phi'_i \; d\Omega$ which appears in the fine scales' energy equation in Eqs. (11) is not modeled as for high Reynolds numbers and low Mach values, its effect can be assumed to be small compared to the previous effect.

Using the modeling described above, Eqs. (10) and Eqs. (11) are combined and transformed into the following modeled system

$$\left\{\begin{array}{ll}
\displaystyle\int_\Omega \frac{\partial\rho}{\partial t}\mathcal{X}_i \; d\Omega + \int_{\partial Sup\mathcal{X}_i} \rho\mathbf{u}.\mathbf{n}\mathcal{X}_i \; d\Gamma & = 0 \\
\displaystyle\int_\Omega \frac{\partial\rho\mathbf{u}}{\partial t}\mathcal{X}_i \; d\Omega + \int_{\partial Sup\mathcal{X}_i} \rho\,\mathbf{u}\otimes\mathbf{u}\,\mathbf{n}\mathcal{X}_i \; d\Gamma + \int_{\partial Sup\mathcal{X}_i} P\mathbf{n}\mathcal{X}_i \; d\Gamma & \\
\displaystyle + \int_\Omega \sigma\nabla\Phi_i \; d\Omega + \int_\Omega \tau'\nabla\Phi'_i \; d\Omega & = \mathbf{0} \\
\displaystyle\int_\Omega \frac{\partial E}{\partial t}\mathcal{X}_i \; d\Omega + \int_{\partial Sup\mathcal{X}_i} (E+P)\mathbf{u}.\mathbf{n}\mathcal{X}_i \; d\Gamma + \int_\Omega \sigma\mathbf{u}.\nabla\Phi_i \; d\Omega & \\
\displaystyle + \int_\Omega \lambda\nabla T.\nabla\Phi_i \; d\Omega + \int_\Omega \frac{C_p\mu'_t}{Pr_t}\nabla T'.\nabla\Phi'_i \; d\Omega & = 0
\end{array}\right. \tag{23}$$

5 Upwinding with sixth-order spatial viscosity

As stated in Section 2, in this work the convective terms are semi-discretized by a FV method. More specifically, Roe's scheme [17] is used together with a MUSCL approach [14, 15] in which stabilization is obtained by a numerical diffusion based on sixth-order derivatives [13]. Such a dissipation has a very localized effect on high frequencies, which reduces its interaction with the subgrid scale modeling as shown in [18]. This improved numerical dissipation is an important component of the resulting numerical scheme for LES,

as it reduces the competition with the modeling role of the LES terms and increases the efficiency of filtering the very fine scales.

Let $V(i)$ denote the set of neighboring nodes to vertex i, and let

$$\mathcal{F}(\mathbf{W}) = (\rho\mathbf{u}, \rho\mathbf{u} \otimes \mathbf{u}, (E+P)\mathbf{u})^t \tag{24}$$

where the superscript t denotes the transpose. The convective fluxes

$$\int_{\partial C_i} \mathcal{F}(\mathbf{W}).\mathbf{n}\ d\Gamma = \sum_{j \in V(i)} \int_{\partial C_i \cap \partial C_j} \mathcal{F}(\mathbf{W}).\mathbf{n}\ d\Gamma$$

are approximated by the numerical fluxes $\sum_{j \in V(i)} \Phi(\mathbf{W}_{ij}, \mathbf{W}_{ji}, \mathbf{n}_{ij})$ where $\mathbf{n}_{ij} = \int_{\partial C_i \cap \partial C_j} \mathbf{n}\ d\Gamma$ and

$$\Phi(\mathbf{W}_{ij}, \mathbf{W}_{ji}, \mathbf{n}_{ij}) = \frac{\mathcal{F}(\mathbf{W}_{ij}, \mathbf{n}_{ij}) + \mathcal{F}(\mathbf{W}_{ji}, \mathbf{n}_{ij})}{2} - \gamma \mathbf{d}(\mathbf{W}_{ij}, \mathbf{W}_{ji}, \mathbf{n}_{ij}). \tag{25}$$

The upwind term is given by

$$\mathbf{d}(\mathbf{W}_{ij}, \mathbf{W}_{ji}, \mathbf{n}_{ij}) = |R(\mathbf{W}_{ij}, \mathbf{W}_{ji}, \mathbf{n}_{ij})| \frac{\mathbf{W}_{ji} - \mathbf{W}_{ij}}{2}\ . \tag{26}$$

The state vectors $\mathbf{W}_{ij}$ and $\mathbf{W}_{ji}$ are reconstructed values of $\mathbf{W}$ at the boundary $\partial C_i \cap \partial C_j$ between the two cells centered at nodes i and j

$$\begin{aligned} \mathbf{W}_{ij} &= \mathbf{W}_i + \tfrac{1}{2}(\nabla \mathbf{W})_{ij}.\vec{ij} \\ \mathbf{W}_{ji} &= \mathbf{W}_j - \tfrac{1}{2}(\nabla \mathbf{W})_{ji}.\vec{ij}. \end{aligned}$$

The gradient $(\nabla \mathbf{W})_{ij}.\vec{ij}$ is computed by

$$\begin{aligned} (\nabla \mathbf{W})_{ij}.\vec{ij} = \quad & (1-\beta)(\nabla \mathbf{W})^C_{ij}.\vec{ij} + \beta(\nabla \mathbf{W})^U_{ij}.\vec{ij} \\ & + \xi_c \left[(\nabla \mathbf{W})^U_{ij}.\vec{ij} - 2(\nabla \mathbf{W})^C_{ij}.\vec{ij} + (\nabla \mathbf{W})^D_{ij}.\vec{ij} \right] \\ & + \xi_d \left[(\nabla \mathbf{W})_M.\vec{ij} - 2(\nabla \mathbf{W})_i.\vec{ij} + (\nabla \mathbf{W})_j.\vec{ij} \right] \end{aligned} \tag{27}$$

where
$(\nabla \mathbf{W})^U_{ij}$ = gradient in the upwind tetrahedron T_{ij} (see Fig. 3)
$(\nabla \mathbf{W})^D_{ij}$ = gradient in the downwind tetrahedron T_{ji} (see Fig. 3)
$(\nabla \mathbf{W})_i$ = nodal gradient for cell C_i
$(\nabla \mathbf{W})_j$ = nodal gradient for cell C_j
$(\nabla \mathbf{W})^C_{ij}$ = centered gradient: $(\nabla \mathbf{W})^C_{ij}.\vec{ij} = \mathbf{W}_j - \mathbf{W}_i$
M=intersection point between the opposite face to vertex i in the upwind tetrahedron T_{ij}

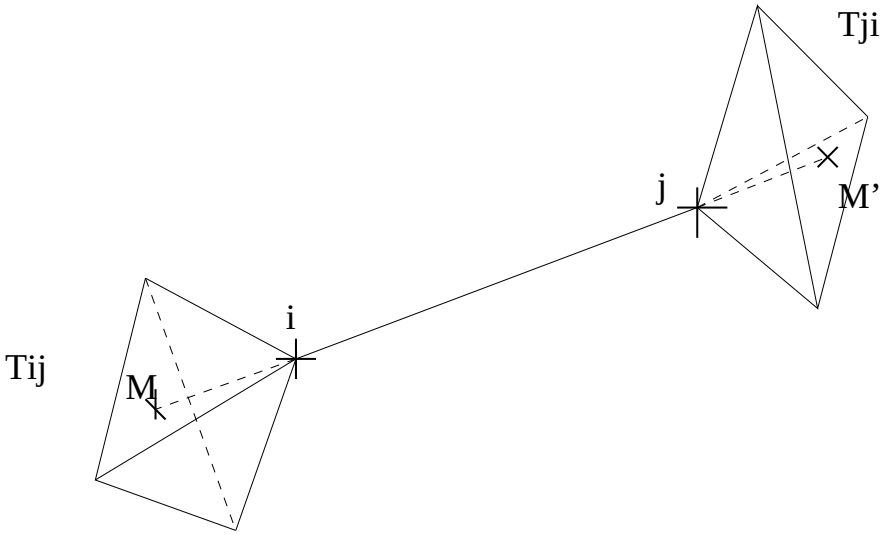

Figure 3: Location of interpolation points M and M', and tetrahedra T_{ij} and T_{ji}

and segment ij (see Fig. 3)
$(\nabla \mathbf{W})_M$ = gradient at point M computed by interpolating the nodal gradients of the vertices located on the opposite face to vertex i in the upwind tetrahedron T_{ij}.

The same approach is used for evaluating $(\nabla \mathbf{W})_{ji}.\vec{ij}$.

In order to have an upwind stabilization term involving a sixth-order spatial viscosity, the values of the upwinding parameters β, ξ_c and ξ_d are set to [13]

$$\beta = \frac{1}{3}, \quad \xi_c = -\frac{1}{30}, \quad \xi_d = -\frac{2}{15}.$$

The positive parameter γ is chosen to be less or equal to 1. It controls directly the upwind term of the numerical fluxes. In practice, this parameter is set to a small value not only to reduce the competition between the spatial numerical dissipation and the dissipation of the LES model, but also to eliminate unphysical pressure oscillations.

6 Time discretization

After semi-discretization, the modeled system (23) can be written for each control volume C_i as

$$Vol(C_i)\frac{d\mathbf{W}_i}{dt} + F_i(\mathbf{W}) + R_i^l(\mathbf{W}) + R_i^t((I-P)(\mathbf{W})) = 0 \tag{28}$$

where $F_i(\mathbf{W})$ represents the semi-discrete convective fluxes $\sum_{j\in V(i)} \Phi(\mathbf{W}_{ij}, \mathbf{W}_{ji}, \mathbf{n}_{ij})$ defined by Eqs. (25-27), and $R_i^l(\mathbf{W})$ and $R_i^t(\mathbf{W}')$ denote the semi-discrete laminar and turbulent diffusive fluxes

$$\sum_{\mathrm{T,i}\in\mathrm{T}} \int_{\mathrm{T}} (0, \sigma\nabla\Phi_i, (\sigma\mathbf{u} + \lambda\nabla T).\nabla\Phi_i)^t \; d\Omega$$

and

$$\sum_{\mathrm{T,i}\in\mathrm{T}} \int_{\mathrm{T}} \left(0, \tau'\nabla\Phi_i', \frac{C_p\mu_t'}{Pr_t}\nabla T'.\nabla\Phi_i\right)^t \; d\Omega,$$

respectively.

The explicit time-integration of Eq. (28) is straightforward. In this work, it is carried out by the following four-step Runge-Kutta algorithm

$$\begin{aligned}
&\mathbf{W}_i^{(0)} = \mathbf{W}_i^n \\
&\mathbf{W}_i^{(k)} = \mathbf{W}_i^{(0)} - \alpha_k \frac{\Delta t^n}{Vol(C_i)} \left(F_i(\mathbf{W}^{(k-1)}) + R_i^l(\mathbf{W}^{(k-1)}) + R_i^t((I-P)(\mathbf{W}^{k-1}))\right) \;, k = 1, \cdots, 4 \\
&\mathbf{W}_i^{n+1} = \mathbf{W}_i^{(4)}
\end{aligned}$$

where $\alpha_1 = 0.11$, $\alpha_2 = 0.2766$, $\alpha_3 = 0.5$ and $\alpha_4 = 1$.

The implicit time-integration of Eq. (28) requires in principle a linearization involving the Jacobians $\frac{\partial F_i}{\partial \mathbf{W}}(\mathbf{W}^n)$, $\frac{\partial R_i^l}{\partial \mathbf{W}}(\mathbf{W}^n)$, and $\frac{\partial R_i^t}{\partial \mathbf{W}}((I-P)(\mathbf{W}^n))$. Constructing second-order approximations of these three Jacobians is a complex but feasible task (for example, see [19]). Alternatively, a defect-correction procedure [20] in which each Jacobian matrix is constructed from the linearization of a first-order approximation method, or a Newton-Krylov [21] approach in which these Jacobians are approximated by finite differencing second-order fluxes can be chosen for solving at each time-step the resulting linearized system of equations. A simpler computational strategy consists in adopting a semi-implicit approach in which the turbulent diffusive fluxes are evaluated at the time-instance t^n — that is, discretizing Eq. (28) by

$$Vol(C_i)\frac{d\mathbf{W}_i^{n+1}}{dt} + F_i(\mathbf{W}^{n+1}) + R_i^l(\mathbf{W}^{n+1}) + R_i^t((I-P)(\mathbf{W}^n)) = 0$$

and applying an existing technique for linearizing the convective and laminar diffusive fluxes.

7 The square cylinder benchmark problem

As a validation problem, the flow past a square cylinder at the Mach number $M_\infty = 0.1$ and Reynolds number $Re = 22,000$ is considered here. This flow was investigated experimentally by several research teams [22, 23, 24, 25, 26], and simulated numerically using both LES simulations [27, 28, 29] and Reynolds Averaged Navier-Stokes (RANS) models [30].

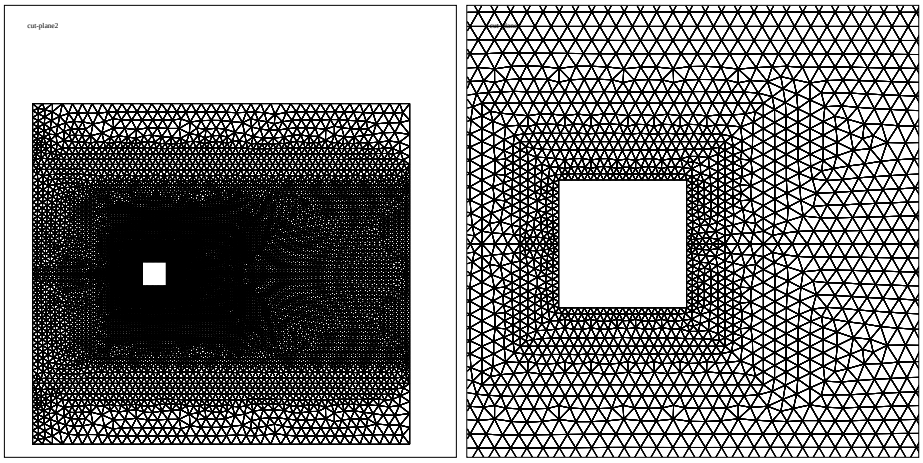

Figure 4: Computational domain: vertical cut-plane of the mesh, and zoom around the square cylinder

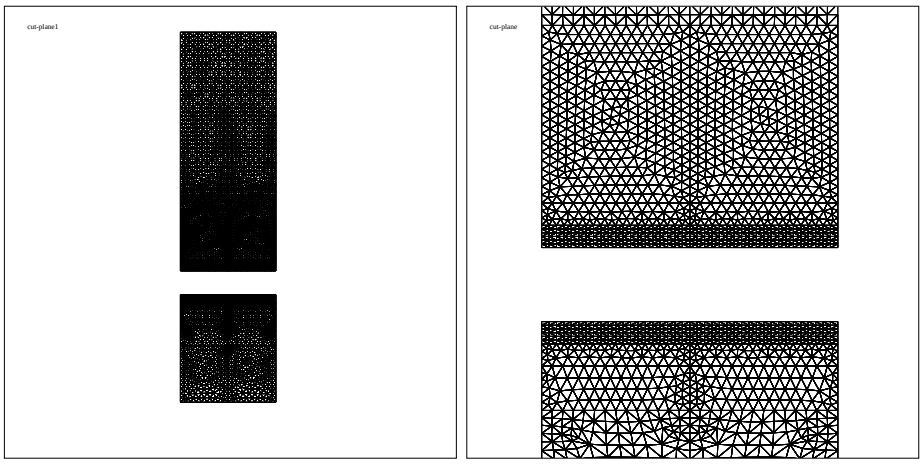

Figure 5: Computational domain: horizontal cut-plane of the mesh, and zoom around the square cylinder

For the purpose of VMS-LES simulations, the computational domain shown in Fig. 4 and Fig. 5 is adopted with

$$\frac{L_i}{D} = 4.5, \ \frac{L_o}{D} = 9.5, \ \frac{L_s}{D} = 4, \text{ and } \frac{H}{D} = 6.5.$$

Here, D denotes the side length of the square cylinder, L_i and L_o are the distances between the cylinder and the inflow and outflow boundaries, respectively, L_s denotes the width of the cylinder (spanwise direction), and H is the distance between the cylinder and the domain boundaries located above and below it. The size of this computational domain is similar to the sizes used in the LES workshop [27] except for a smaller L_o.

This computational domain is discretized by 200,000 nodes and 1,100,000 tetrahedra. Horizontal and vertical cut-planes of the unstructured mesh are shown in Fig. 4 and Fig. 5. In the spanwise direction, approximately 40 nodes are used near the cylinder, which corresponds to a spanwise resolution $\Delta z \simeq 0.1D$. The average distance of the closest points to the cylinder wall is $0.05\,D$, which corresponds to $y^+ \simeq 10 - 80$. This distance is rather large compared to that typically used in LES.

The boundary conditions at the wall are enforced through Reichardt's wall law [31] to avoid a very fine discretization near the wall. For the lateral sides of the computational domain we use periodic boundary conditions, and slip conditions are imposed on the horizontal sides located above and below the cylinder. The inflow and outflow boundaries are treated by the Steger-Warming flux decomposition [32]. Finally, the upwind parameter γ is set to 0.2.

Two different VMS-LES simulations are performed for a preliminary investigation of the effect of the size of the macro-cells. Hence, these simulations differ only by the specifics of the algorithm used to construct the macro-cells. In VMS-LES (2), the macro-cells are larger than in VMS-LES (1). The main bulk quantities predicted by these simulations are reported in Table 1 together with those obtained with the classical LES method (same code as the present VMS-LES code but without the VMS formulation), and contrasted with the results obtained by other LES simulations and experiments. All simulations performed in this work are for 10 periods of vortex shedding, using the four-step Runge-Kutta explicit scheme with a time-step corresponding to sampling the main period in 2,700 time steps. The notation used in Table 1 is as follows: $\overline{C}_d$ is the mean drag coefficient, C'_d is the root mean square (r.m.s.) of the drag coefficient, C'_l is the r.m.s. of the lift coefficient, St is the Strouhal number, l_r is the recirculation length behind the square cylinder, and $\overline{C}_{p_b}$ is the mean pressure coefficient on the rear face of the square cylinder at $y = 0$. Here, the computed Strouhal number is obtained from a Fourier analysis of the lift coefficient (see Fig. 8). Instantaneous contourplots of the Mach number are also shown in Fig. 6 and Fig. 7. These plots highlight the small structures predicted in the wake by the rather coarse mesh employed in this work, and the three dimensionality of the flow.

The results displayed in Table 1 show that the VMS formulation improves the prediction by LES of most reported bulk quantities, in particular the mean drag coefficient, the mean

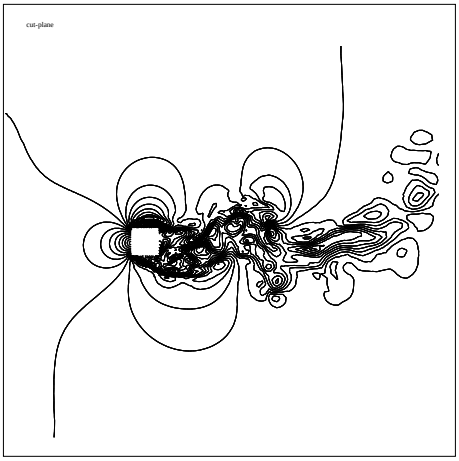

Figure 6: Instantaneous Mach field in a vertical plane

Figure 7: Instantaneous Mach field in a horizontal plane

LES	$\overline{C_d}$	C'_d	C'_l	S_t	l_r	$-\overline{C}_{p_b}$
VMS-LES (1)	2.10	0.17	0.98	0.134	1.4	1.48
VMS-LES (2)	2.10	0.18	1.08	0.136	1.4	1.52
Classical LES	2.00	0.19	1.01	0.136	1.5	1.31
Rodi *et al.* [27]	[1.66,2.77]	[0.10,0.27]	[0.38,1.79]	[0.07,0.15]	[0.89,2.96]	-
Sohankar *et al.* and Fureby et al. [29, 28]	[2.00,2.32]	[0.16,0.20]	[1.23,1.54]	[0.127,0.135]	[1.29,1.34]	[1.30-1.63]
Experiments	$\overline{C_d}$	C'_d	C'_l	S_t	l_r	$-\overline{C}_{p_b}$
Lyn *et al.* [24, 25]	2.10	-	-	0.132	1.4	-
Luo *et al.* [26]	2.21	0.18	1.21	0.13	-	1.52
Bearman *et al.* [22]	2.28	-	1.20	0.13	-	1.60

Table 1: Bulk coefficients predicted by various LES simulations and comparison with experimental data (a pair of brackets designate a range between extreme values)

pressure coefficient on the rear face of the cylinder, and the recirculation length behind the cylinder. All quantities but the r.m.s. of the lift coefficient are well predicted (with a relative error smaller than 4 %) by the VMS-LES simulations. The size of the macro-cells does not appear to have a clear effect on the quality of the results. All simulations appear to underestimate the r.m.s. of the lift coefficient, perhaps because of an insufficient grid quality or resolution near the cylinder and the use of a wall law.

Fig. 9 displays the profiles of the time-averaged streamwise velocity u_x in the center of the wake predicted by the LES and VMS-LES methods, and contrasts them with the experimental data [24, 25]. For $x \leq 1.8D$ in the wake, the VMS formulation improves significantly the result predicted by the classical LES method. For $x > 3D$, all simulation results (as well as other LES results published in [27, 28, 29] for this same problem) overestimate the recovery of the streamwise velocity. Nevertheless, the results predicted by the VMS-LES (1) are the closest to the experimental data.

Fig. 10 shows the profiles of the time-averaged streamwise velocity u_x along a vertical cut located in the half domain above the square cylinder at a distance $x = 0.25D$ from the middle point of its upper face. For $x \leq 0.8D$, the improvement brought by the VMS formulation to the LES method is clearly demonstrated. For $x > 0.8D$, the results delivered by all LES methods correlate well with the experimental data [24, 25].

Fig. 11 reports on the distribution of the time-averaged pressure coefficient along the upper-half of the square. Here, AB designates the upper-half front face of the cylinder, BC its upper face, and CD its upper-half rear face. The experimental data is that reported in [22]. All LES results appear to correlate well with the experimental data on face AB, and to underestimate the mean pressure coefficient on face BC. On the rear face CD, the VMS-LES method delivers better results than the classical LES method.

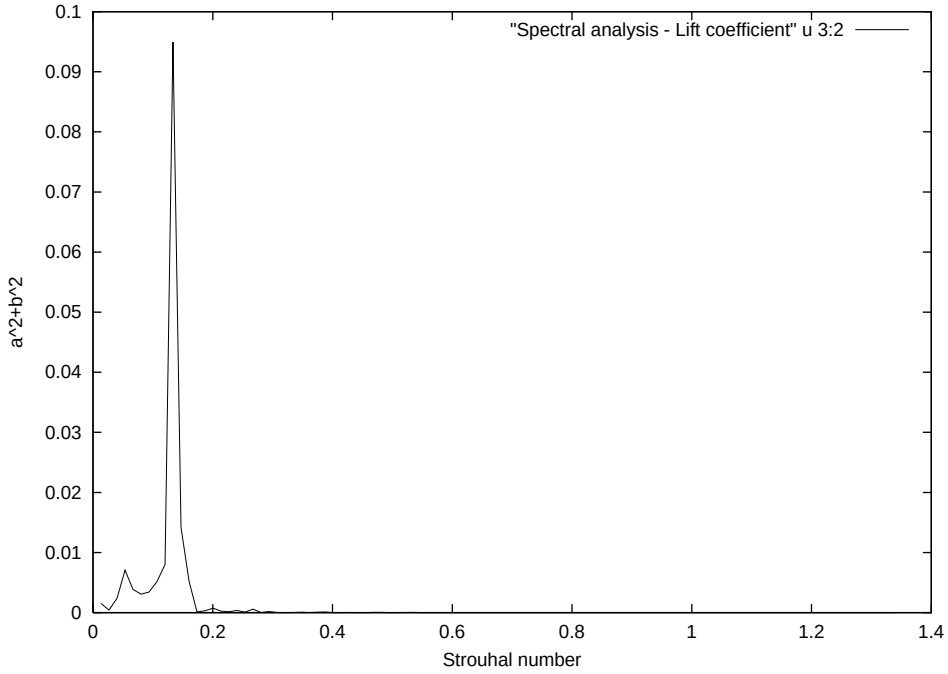

Figure 8: Spectral analysis of the lift coefficient

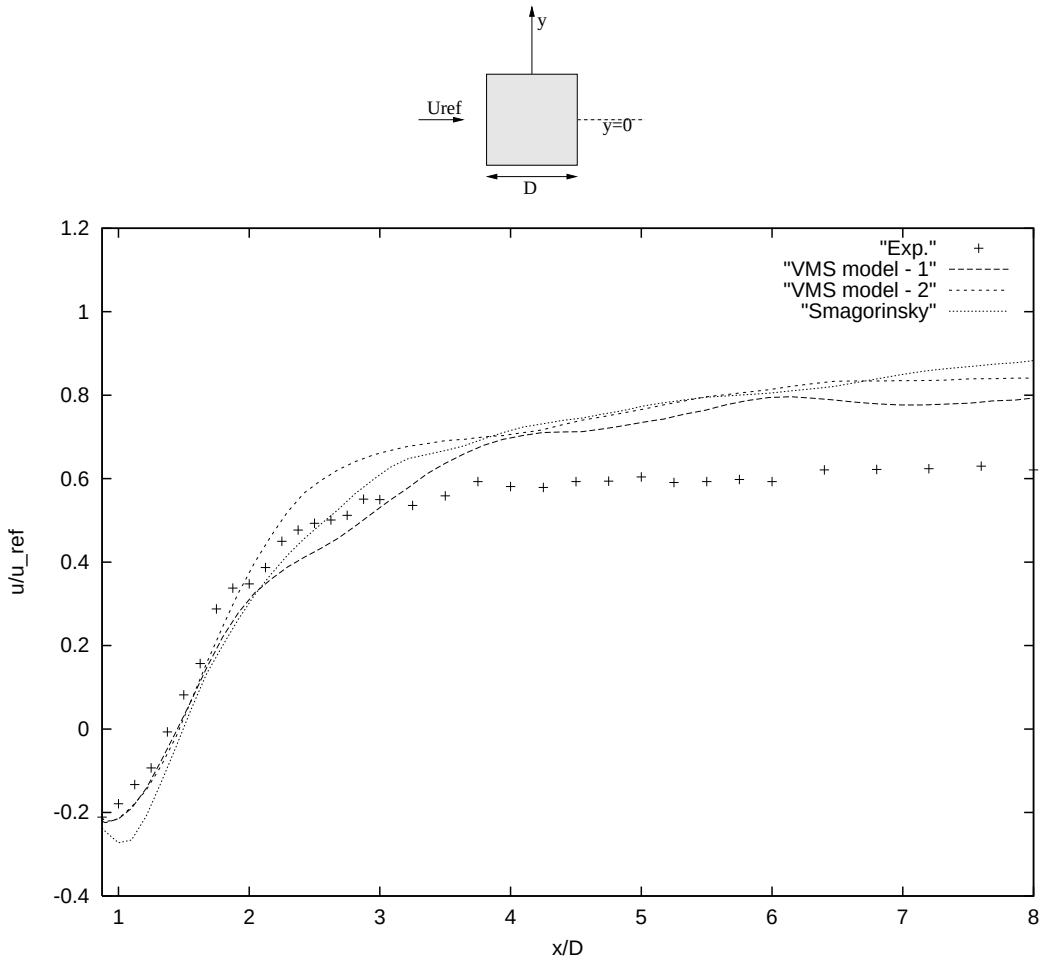

Figure 9: Profile of the mean streamwise velocity in the center of the wake

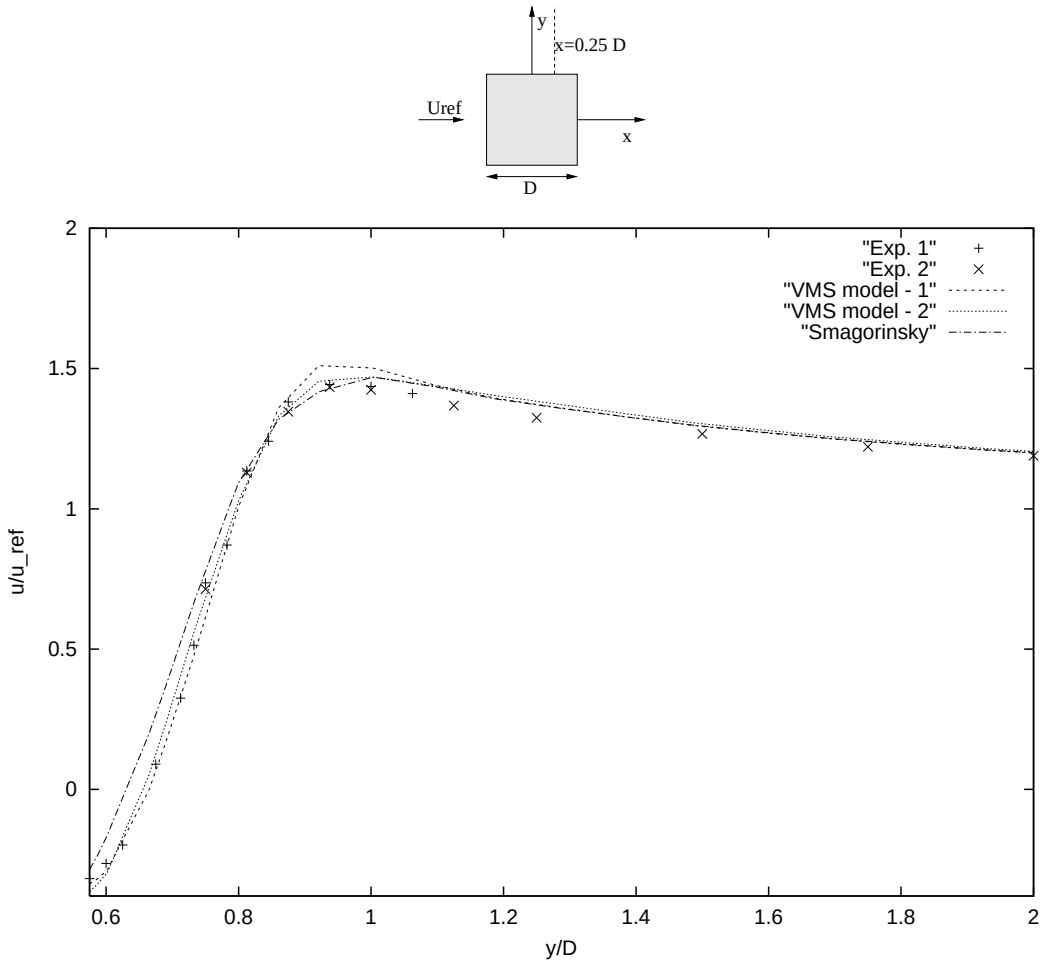

Figure 10: Profile of the mean streamwise velocity at $x = 0.25D$

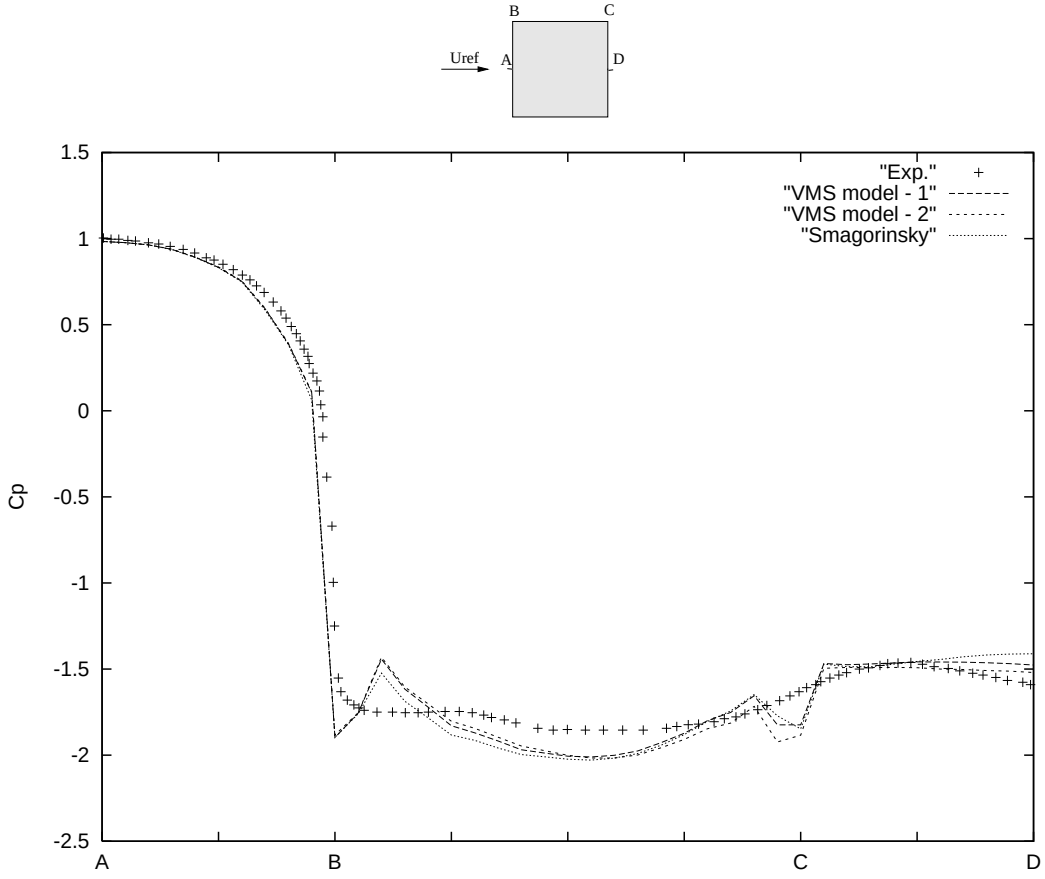

Figure 11: Mean pressure coefficient distribution along the upper-half of the cylinder

8 Conclusion

A finite volume/element discretization on tetrahedral meshes of the variational multiscale formulation of large eddy simulations for turbulent compressible flows was presented. Its key features are an economical procedure based on cell agglomeration for separating a priori the scales, and an effective strategy for controling the numerical dissipation induced by upwinding so that it does not interfere with the subgrid scale modeling. The resulting LES method was equipped with Reichardt's wall law and validated with the three-dimensional numerical simulation of a vortex shedding flow past a square cylinder at $M_\infty = 0.1$ and $Re = 22{,}000$. Even though a coarse mesh was used for this purpose, the computed drag coefficient and its root mean square (r.m.s.), Strouhal number, recirculation length and mean pressure coefficient on the rear face of the cylinder correlate well with their measured counterparts, and are more accurate than those predicted by the classical large eddy simulation method using the same grid.

Acknowledgements

The authors would like to thank A. Dervieux, S. Camarri, M.V. Salvetti and T. Hughes for many enlightening discussions on LES and VMS. The first author is also grateful to CINES (Centre Informatique National de l'Enseignement Supérieur) for providing computational facilities.

References

[1] J. Smagorinsky, General circulation experiments with the primitive equations, Mon. Weather Rev, 91, 99-164, 1963.

[2] M. Germano, U. Piomelli, P. Moin and W.H. Cabot, A dynamic subgrid-scale model, Phys. Fluids, A3, 1760-1765, 1991.

[3] P. Moin, K. Squires, W. Cabot and S. Lee, A dynamic subgrid-scale model for compressible turbulence and scalar transport, Phys. Fluids, A3, 2746-2757, 1991.

[4] S. Camarri and M.-V. Salvetti, Towards the large-eddy simulation of complex engineering flows with unstructured grids, INRIA report, N^o 3844, 1999.

[5] S. Camarri, M.V. Salvetti, B. Koobus and A. Dervieux,Large-eddy simulation of a bluff-body flow on unstructured grids, to appear in Int. J. Num. Meth. Fluids, 2002.

[6] D.K. Lilly, A proposed modification of the Germano subgrid-scale closure method, Phys. Fluids, A4, 633, 1992.

[7] T.J.R. Hughes, L. Mazzei and K.E. Jansen, Large eddy simulation and the variational multiscale method, Comput. Vis. Sci., 3, 47, 2000.

[8] T.J.R. Hugues, L. Mazzei, A. A. Oberai and A. A. Wray, The multiscale formulation of large eddy simulation: Decay of homogeneous isotropic turbulence, Phys. Fluids, 13, 505-512, 2001.

[9] T.J.R. Hugues, A. A. Oberai and L. Mazzei, Large eddy simulation of turbulent channel flows by the variational multiscale method, Phys. Fluids, 13, 1784-1799, 2001.

[10] K.E. Jansen and A.E. Tejada-Martínez, An evaluation of the hierarchical basis in variational multiscale LES, in: Mang et al. [12].

[11] C. Farhat and B. Koobus, Finite volume discretization on unstructured meshes of the multiscale formulation of large eddy simulations, in: Mang et al. [12].

[12] H.A. Mang, F.G. Rammerstorfer, J.Eberhardsteiner (Eds.), Proceedings of the Fifth World Congress (WCCM V), Vienna University of Technology, Austria, 2002.

[13] C. Debiez and A. Dervieux, Mixed element volume MUSCL methods with weak viscosity for steady and unsteady flow calculation, Comput. & Fluids, 29, 89-118, 1999.

[14] B. Van Leer, Towards the ultimate conservative difference scheme V: a second-order sequel to Godunov's method, J. Comp. Phys., 32, 361-370, 1979.

[15] A. Dervieux, Steady Euler Simulations Using Unstructured Meshes, Von Karman Institute Lecture Series, 1985.

[16] M.H. Lallemand, H. Steve and A. Dervieux, Unstructured multigridding by volume agglomeration: current status, Comput. & Fluids 21, 397-433, 1992.

[17] P.L. Roe, Approximate Riemann solver, parameters vectors and difference schemes, J. Comp. Phys., 43, 357-371, 1981.

[18] S. Camarri, B. Koobus, M.V. Salvetti and A. Dervieux, Numerical diffusion based on high-order derivatives in MUSCL schemes for LES on unstructured grids, DLES-4, Twente, July 18-20, 2001.

[19] M. Lesoinne, M. Sarkis, U. Hetmaniuk, and C. Farhat, A linearized method for the frequency analysis of three-dimensional fluid/structure interaction problems in all flow regimes, Comput. Meths. Appl. Mech. Engrg., 190, 3121-3146, 2001.

[20] K. Bohmer, P. Hemker and H. Stetter, The defect correction approach, Comp. Supp., 5, 1-32, 1984.

[21] D.E. Keyes and V. Venkatakrishnan, Newton-Krylov-Schwarz methods: interfacing sparse linear solvers with nonlinear applications, Zeitschrift für Angewandte Mathematik und Mechanik, 76, 147-150, 1996.

[22] P. Bearman and E. Obasaju, An experimental study of pressure fluctuations on fixed and oscillating square-section cylinders, J. Fluid Mech., 119, 297-321, 1981.

[23] C. Norberg, Flow around rectangular cylinders: pressure forces and wake frequencies, J. Wind Eng. Ind. Aerodyn., 49, 187-196, 1993.

[24] D. Lyn and W. Rodi, The flapping shear layer formed by flow separation from the forward corner of a square cylinder, J. Fluid Mech., 267, 353-376, 1993.

[25] D. Lyn, S. Einav, W. Rodi and J. Park, A laser-doppler velocimeter study of enesemble-averaged characteristics of the turbulent near wake of a square cylinder, J. Fluid Mech., 304, 285-319, 1995.

[26] S. Luo, M. Yazdani, Y. Chew and T. Lee, Effects of incidence and afterbody shape on flow past bluff cylinders, J. Wind Eng. Ind. Aerodyn., 53, 375-399,1994.

[27] W. Rodi, J. Ferziger, M. Breuer and M. Pourquié, Status of large eddy simulations: results of a workshop, ASME J. Fluids Eng., 119, 248-262, 1997.

[28] C. Fureby, G. Tabor, H. Weller and A. Gosman, Large eddy simulation of the flow around a square prism, AIAA J., 38, 442-452, 2000.

[29] A. Sohankar, L. Davidson and C. Norberg, Large eddy simulation of flow past a square cylinder: comparison of different subgrid scale models, ASME J. Fluids Eng., 122, 39-47, 2000.

[30] B. Koobus, H. Tran and C. Farhat, Computation of unsteady viscous flows around moving bodies using the k-ε turbulence model on unstructured dynamic grids, Comput. Meths. Appl. Mech. Engrg., 190, 1441-1466, 2000.

[31] J.O. Hinze, Turbulence, McGraw-Hill, New York, 1959.

[32] J. Steger and R.F. Warming, Flux vector splitting for the inviscid gas dynamic with applications to finite-difference methods, J. Comp. Phys. 40, 263-293, 1981.

Unité de recherche INRIA Sophia Antipolis
2004, route des Lucioles - BP 93 - 06902 Sophia Antipolis Cedex (France)

Unité de recherche INRIA Lorraine : LORIA, Technopôle de Nancy-Brabois - Campus scientifique
615, rue du Jardin Botanique - BP 101 - 54602 Villers-lès-Nancy Cedex (France)
Unité de recherche INRIA Rennes : IRISA, Campus universitaire de Beaulieu - 35042 Rennes Cedex (France)
Unité de recherche INRIA Rhône-Alpes : 655, avenue de l'Europe - 38330 Montbonnot-St-Martin (France)
Unité de recherche INRIA Rocquencourt : Domaine de Voluceau - Rocquencourt - BP 105 - 78153 Le Chesnay Cedex (France)

Éditeur
INRIA - Domaine de Voluceau - Rocquencourt, BP 105 - 78153 Le Chesnay Cedex (France)
http://www.inria.fr
ISSN 0249-6399